Exp Astron
DOI 10.1007/s10686-014-9376-3

ORIGINAL ARTICLE

JEM-EUSO observational technique and exposure

M. Bertaina · P. Bobik · F. Fenu · K. Shinozaki
on behalf of the JEM-EUSO Collaboration

Received: 21 August 2013 / Accepted: 24 February 2014

Abstract Designed as the first mission to explore the ultra-high energy universe from space, JEM-EUSO observes the Earth's atmosphere at night to record the ultraviolet tracks generated by the extensive air showers. We present the expected geometrical aperture and annual exposure in the nadir and tilt modes for ultra-high energy cosmic rays observation as a function of the altitude of the International Space Station.

Keywords JEM-EUSO · Ultra-high energy cosmic rays · Extensive air showers

M. Bertaina (✉)
Dipartimento di Fisica, Università di Torino and INFN Torino, via P. Giuria 1, 10125 Torino, Italy
e-mail: bertaina@to.infn.it

P. Bobik
Department of Space Physics, Institute of Experimental Physics, Watsonova 47, 040 01 Kosice, Slovakia
e-mail: bobik@saske.sk

F. Fenu · K. Shinozaki
Institute for Astronomy and Astrophysics, Kepler Center, University of Tübingen, Sand 1, 72076 Tübingen, Germany

F. Fenu
e-mail: francesco.fenu@gmail.com

K. Shinozaki
e-mail: shinozaki@astro.uni-tuebingen.de

Published online: 27 March 2014

1 Introduction

JEM-EUSO (the Extreme Universe Space Observatory on board the Japanese Experiment Module) [1, 2] is an innovative space-based mission with the aim of detecting Ultra-High Energy Cosmic Rays (UHECRs) from the International Space Station (ISS), by using the Earth's atmosphere as a calorimeter seen by a fluorescence detector. An observatory able to produce an arrival direction map with more than several hundreds events above $\sim 5 \times 10^{19}$ eV would give important information on the origin of the UHECRs and identify structures in the sky map that contain information about the source density and/or distribution. This is likely to lead to an understanding of the acceleration mechanisms perhaps producing discoveries in astrophysics and/or fundamental physics. The comparison of the energy spectra among the spatially resolved individual sources will help to clarify the acceleration and emission mechanisms, and also finally confirm the Greisen-Zatsepin-Kuz'min process [3, 4] for the validation of Lorentz invariance up to Lorenz factor of $\sim 10^{11}$. This is the main objective of the JEM-EUSO mission. If fluxes are high enough, neutral components, i.e. neutrinos and gamma rays, may be also detected [5].

JEM-EUSO consists of a UV telescope and an atmospheric monitoring system. Orbiting the Earth every $\sim$ 90 minutes at an altitude of $H_{\rm ISS} \sim 400$ km from the Earth's surface,[1] JEM-EUSO is designed to detect UV (300–430 nm) fluorescence photons produced along the track of Extensive Air Showers (EASs) in the atmosphere. The main telescope has a wide Field-of-View (FoV; ~ 0.85 sr) optics composed of three Fresnel lenses. The results presented in this paper assume the 'side-cut' version of the instrument with a 2.65 m diameter on the major axis and 1.9 m on the minor one (4.5 m^2 optical aperture) to fit in the cargo of the JAXA HTV rocket as described in Ref. [6]. The telescope records the EAS-induced tracks with a time resolution of 2.5 μs (Gate Time Unit; GTU). The Focal Surface (FS) detector is formed by 137 Photo Detector Modules (PDMs) composed of $\sim$ 5000 Multi-Anode Photo-Multiplier Tubes (MAPMTs) in total (36 MAPMT per PDM, 64 pixels each). The FS detector is highly pixelated in $\sim 3 \times 10^5$ channels providing a spatial resolution of $\sim 0.074°$, equivalent to $\sim$ 0.5 km at ground seen from an altitude of $\sim$400 km. An optical filter is placed in front of the MAPMTs to select photons in the fluorescence bandwidth (see Table 1 for a detailed list of JEM-EUSO instrumental parameters). These time-segmented images allow the measurement of the energy and arrival direction of the primary particles.

Since the ISS orbits the Earth in the latitude range of $\pm 51.6°$, moving at a speed of ~ 7.6 km s^{-1}, the variability of the FoV observed by JEM-EUSO is much higher than that observed by ground-based experiments. In particular, the atmospheric conditions, which eventually determine the aperture, must be carefully monitored via the atmospheric monitoring system consisting of an infrared camera and a steerable laser [7]. A Global Light System (GLS) consisting of a network of ground-based xenon flashlamps and steered UV lasers is also foreseen to validate the key functions of the JEM-EUSO detector such as triggers, accuracy of energy and direction

[1] Hereafter, Earth's surface is referred to as the assumed Earth's ellipsoid model and the altitude is measured from this level.

Table 1 Parameters of the JEM-EUSO telescope [6]. The values in parentheses apply at the edge of the FoV, otherwise at the the center of the FoV. The ensquared collection efficiency is the ratio of the number of photons focused within a pixel area to those incident on the entrance aperture of the optics. The ensquared energy is the ratio of photons focused within the area of a pixel to those reaching the photo-detector on the FS

Parameter	Value	Note
Optics		
Optical aperture	4.5 m^2	baseline
Ensquared collection efficiency	35% (15%)	for λ = 350 nm
Ensquared energy	86% (80%)	for λ = 350 nm
Optical bandwidth	300–430 nm	
Field of view	0.85 sr	
Observational area (nadir mode)	1.4×10^5 km^2	for $H_{ISS} = 400$ km
FS detector and electronics		
Number of pixels	3.2×10^5	
Spatial angular resolution	0.074°	
Pixel size at ground	0.51 km (0.61 km)	for $H_{ISS} = 400$ km
Quantum efficiency	41%	for $\lambda = 350$ nm
Collection efficiency	80%	
Cross talk	$< 2\%$	
Transmittance of UV filter	97%	for λ = 350 nm
Sampling time (GTU)	2.5 μs	

reconstruction. In the present configuration, which assumes 12 GLS stations spread on continents and islands, typically, but not only, remote science facilities, the average time difference between two successful measurements is ∼2 days [8].

In the following, we describe fundamental principles of JEM-EUSO, including the peculiarity of the space-based observation of EASs (Section 2). We also discuss key parameters relevant to the performance of the JEM-EUSO telescope (Section 3). In this work, we evaluate the geometrical aperture (Sections 4 and 5) and expected exposure (Section 6) in various observational conditions based on the trigger efficiency and on fiducial cuts on shower maximum for cloudy conditions. Event reconstruction is not taken into account, however, it is briefly mentioned in Section 7, while a detailed discussion is reported in dedicated articles in this special issue [9, 10].

2 Observational principle

The space-based observation of UHECRs has some peculiarities in comparison to ground-based measurements. Above all, by observing from ∼ 400 km altitude, JEM-EUSO significantly enhances the aperture compared to any existing and planned observatory. In addition to looking vertically down to the nadir (nadir mode), the JEM-EUSO telescope may be tilted astern (tilt mode) to increase the observation area in order to explore even rarer events at the highest energies. Thanks to the ISS

orbit, JEM-EUSO surveys the whole celestial sphere with a rather uniform exposure, minimizing the systematic uncertainties. This is not the case for ground-based observatories that may only observe a limited part of the celestial sky.

There are other interesting aspects in using a space-based UHECR observatory. The limited uncertainty in the distance $L \sim 400$ km to the EAS helps to simplify the observational requirements. The altitude of showers maximum $H_{\max}$ is located at 7 ± 5 km for most of cases [6]. Therefore, even without any information about L, the uncertainty of the brightness B of EAS due to that of extinction loss in high atmosphere is to an order of ~ 20 %, while it doesn't exceed 3 % due to an unknown distance, following $\Delta B/B \propto 2 \cdot \Delta L/L$. On the other hand, when the highest energy showers are seen from ground, without stereo or hybrid observation, the proximity effect is more relevant as the landing position of the shower is not determined precisely. Moreover, the role of aerosols which are abundant in the planetary boundary layer, affect significantly the observation from ground, as the showers are seen through a few atmosphere equivalent depths. Finally, works in the past proved the feasibility of reconstructing EAS with reasonable uncertainty in the presence of clouds [1, 11]. Compared to ground-based detectors, the cloud impact is less relevant to the determination of the exposure.

The JEM-EUSO observational approach mainly relies on the fact that a substantial fraction of the UV fluorescence light generated by the EAS can reach a light-collecting device of several square meters located at several hundreds kilometers away. Typically several thousands of photons reach the JEM-EUSO detector for a shower produced by a 10^{20} eV particle. JEM-EUSO is designed to record not only the number of photons but also their direction and arrival time. It is the measurement of the specific space-time correlation of the signal that helps to identify EAS tracks in the night-glow background.

In order to investigate the shower properties and the detector response, we employ the software package ESAF (EUSO Simulation and Analysis Framework) [12]. Details of the shower simulation, as well as, those of the detector and reconstruction performances are described in [6, 9, 10]. The top panel of Fig. 1 shows the tracks projected on the Earth's surface for EASs with an energy $E = 10^{20}$ eV and zenith angles Θ of a) 30°, b) 60° and c) 75° along with the map for the entire FoV indicated in the inset. The bottom panel shows the image on the FS detector for the case b) in which the integrated counts for each pixel are indicated. The regions enclosed by thick dashed lines in both panels refer to the same PDM. Figure 2 shows the arrival time distribution of photons at the telescope entrance aperture from the EASs shown in Fig. 1. The shaded histogram is for $\Theta = 60°$ and those with solid and dashed lines are for $\Theta = 30°$ and 75°, respectively. Up to zenith angles $\sim 60°$, the EAS has a size comparable to the FoV of 1 PDM, which corresponds to about 30 km on a side, i.e. ~ 1000 km^2 in area for $H_{\rm ISS} = 400$ km. The EAS reaches the FoV of two PDMs around $\Theta \sim 75°$. This is the reason why the trigger architecture is based on the PDM scale, which also means that the entire FS detector can be considered as the sum of 137 quasi-independent sub-detectors corresponding to PDMs. This is important for evaluating the role of clouds and anthropogenic light such as cities on the determination of the exposure. It should be mentioned here that when a trigger is issued on a PDM, the data of the neighboring PDMs are also retrieved.

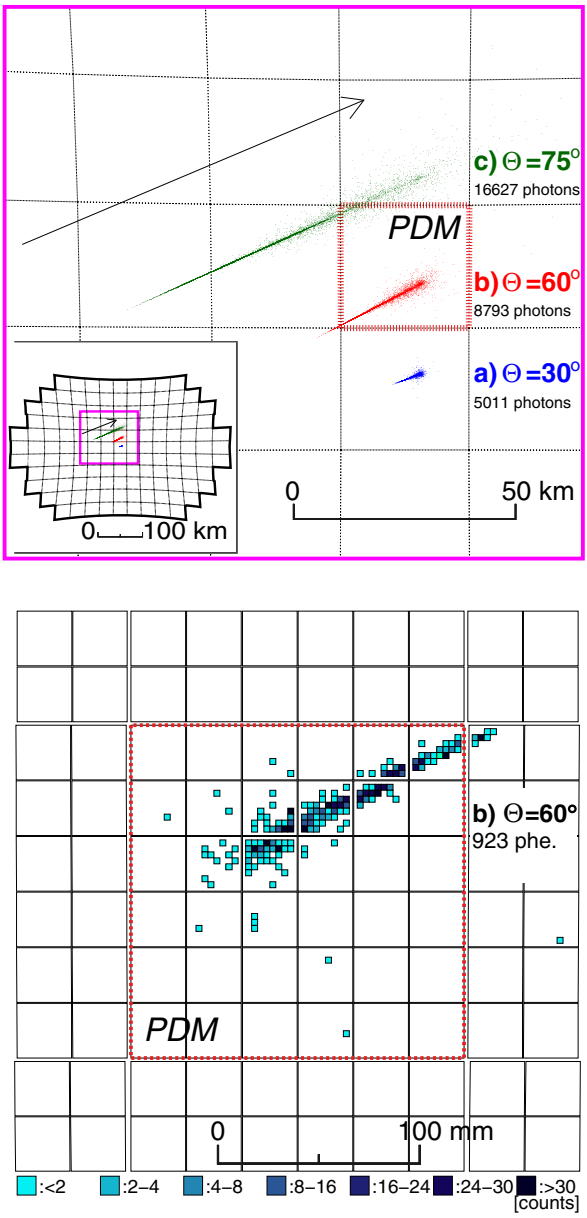

Fig. 1 Top panel shows the projected tracks on the Earth's surface for EASs with $E = 10^{20}$ eV and zenith angles Θ of a) 30°, b) 60° and c) 75°. The dashed lines indicate the corresponding areas for the FoV of individual PDMs. In the inset, the corresponding area of the plot is represented by solid lines within the entire FoV. Each point in the panel and the inset denotes the origin of the arrival photon to JEM-EUSO projected on the Earth's surface. Therefore, each image corresponds to the visible part of the shower development. The density of dots reflects the rate of photon emission and scattering convolved with transmission between shower position and JEM-EUSO. The bottom panel shows the image on the FS detector for the case b). The real image is inverted compared to the above panel, because the shower is located at infinite distance compared to the focal length of the telescope. The large squares denote MAPMTs. The matrix of pixels are indicated with the integrated counts in discrete scale. The regions enclosed by thick dashed lines in both panels refer to the same PDM

Another important consideration is that more inclined EASs give brighter signals at EAS maximum and total integrated light. This can be used to extend the energy range of measurement to lower energies by simple geometrical cuts. Moreover, inclined showers allow almost full calorimetric measurement of the EAS because the entire profile is visible. This is generally not the case of ground-based detectors,

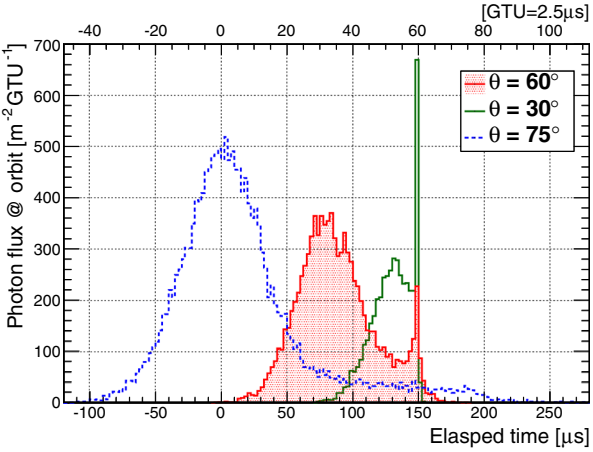

Fig. 2 Arrival time distribution of photons at the telescope entrance from the same EASs shown in Fig. 1. The shaded histogram denotes the case of $\Theta = 60°$ and those with solid and dashed lines are for the cases of $\Theta = 30°$ and $\Theta = 75°$, respectively. The peak around 150 μs is the Cherenkov light hitting the Earth's surface and reflected to the telescope. The three showers are displayed by synchronizing the GTU of the Cherenkov mark. Showers with higher zenith angles are longer and brighter

which typically select events up to 60° in zenith angles, and for which the EAS is truncated at ground in many cases.

3 Observational duty cycle, local light effects and the role of clouds

The estimation of the exposure of a space-based experiment such as JEM-EUSO requires accounting for: a) the characteristics of the EAS development in the atmosphere as observed from space, b) the properties of the telescope, including its orbit and FoV, c) the various sources of 'steady' background like night-glow and moonlight, d) the overall optical transmission properties of the atmosphere, in particular the possible presence of clouds, and e) the effect of anthropogenic light, or other light sources such as Transient Luminous Events (TLEs) and meteors. Topics a) and b) are the principal factors determining the threshold in energy and maximum aperture of the telescope. Topic c) limits the observational duty cycle of the mission. Topics d) and e) affect the instantaneous aperture of the telescope.

The role of each of the above listed aspects has been studied in the past to evaluate their contribution to the determination of the JEM-EUSO exposure. A detailed description of such studies are reported in Ref. [6]. In the following, we summarize the methods and the conclusions there derived. The discussion on the UV emission due to direct particles interacting in the detector is a new topic.

The first aspect is the estimation of the observational duty cycle of JEM-EUSO, or the fraction of time in which the EAS measurement is not hampered by the brightness of the atmosphere. This is mainly due to night-glow and back-scattered moonlight. This value is variable over time. We define the observational duty cycle as the fraction of time η_0 in which the background intensity I_{BG} is lower than a given value

$I_{\mathrm{BG}}^{\mathrm{thr}}$. The moonless condition is assumed to be I_{BG} = 500 photons m^{-2} sr^{-1} ns^{-1} in the range of $\lambda = 300 - 400$ nm [13–15] that produces a signal of $\sim$ 1 photo-electron pixel^{-1} GTU^{-1}. In the present study, we use $I_{\mathrm{BG}}^{\mathrm{thr}}$ = 1500 photons m^{-2} sr^{-1} ns^{-1}. In this condition, the signal-to-noise ratio of a 10^{20} eV shower is still 5 around shower maximum. The back-scattered moonlight is calculated from the moon phase and its apparent position as seen from the ISS. The ISS trajectory provided by NASA SSCweb in the period 2005–2007 is used. The zenith angle of the Sun is required to be greater than 109° for an orbiting altitude of 400 km. The observational duty cycle η_0 ($I_{\mathrm{BG}} < I_{\mathrm{BG}}^{\mathrm{thr}}$) yields to of the order of $\sim$20 %. This value is conservative at energies $E \gtrsim 10^{20}$ eV where it is possible to also operate in higher background levels. The average background level will be monitored constantly by the JEM-EUSO trigger system with a precision of a few percent at PDM level. In the case of a trigger the data of at least 9 PDMs will be acquired for at least 128 GTU (= 320 μs). Assuming the standard background configuration of 500 photons m^{-2} sr^{-1} ns^{-1}, the statistical resolution is $\sim$10 % (1 %) at pixel (MAPMT) level. In such a time span the ISS moves by $\sim$2 m, which is 2 orders of magnitude smaller than the pixel linear size imaged at ground, i.e. $\sim$500 m.

Another source of background is the UV emission due to direct particles interacting in the detector, in particular with the lenses, due to their large size and transparency. The UV emission in the detector lenses due to trapped electrons in the center of the South Atlantic Anomaly (SAA), where the flux of particles exceeds by orders of magnitude to the average one, was studied in Ref. [16]. The SPENVIS AE-8 model [17] is used to compute the electron flux in the SAA. A full GEANT4 [18] simulation, incorporating a complete description of JEM-EUSO Fresnel lenses, is performed to evaluate the light emission in the lenses. The result indicates that the flux of photons due to trapped electrons in SAA in non-disturbed magnetosphere is negligible ($\sim$1 %) compared to the standard UV background discussed above. Only in the cases of disturbed magnetosphere, would the electron flux increase up to $\sim$2 orders of magnitude becoming comparable with the night-glow one. However, it has to be remembered that JEM-EUSO is foreseen to fly in 2017–2019 when the amount of disturbances is expected to be not particularly high.

In addition to the diffuse sources of background, there are transient or steady local sources. In the cases of lightning and TLEs, estimates of the reduction in observational duty cycle and instantaneous aperture are performed assuming the rate of events detected by Tatiana satellite [13]. In Ref. [6], a $\sim$ 2 % reduction of the exposure is derived. In such an estimation, we do not take into account the fact that lightning is very often associated with high-altitude clouds. Therefore, some double counting is included when both lightning and cloud inefficiencies are separately taken into account in the estimation of the exposure. This is explicitly done to reinforce the conservation nature of the calculation. To estimate the reduction in observational duty cycle and aperture due to the occurrence of auroras, we used the K_{p} index to describe the geomagnetic activity, as well as, the geomagnetic latitude and longitude of ISS during years 2001 and 2006. These two years were selected as they were close to solar minimum and solar maximum, respectively. In the estimation, it is assumed that no measurement can be performed when the K_{p} index for ISS geomagnetic latitude is equal to or higher than Auroral Boundary

Index [19]. Even in the case of maximum solar activity, the effect is of the level of ~ 1 %.

To evaluate the effect of light sources on the Earth, which are mainly anthropogenic, we use the Defense Meteorological Satellite Program (DMSP) database. Annual averages of light intensities for cloud-free moonless nights are used to estimate the presence of local light along the ISS trajectory. The DMSP data provide the light intensity at every 30-arcsecond grid on latitude and longitude in the wavelength range 350 nm–2 μs. The stationary background is dominated by visible light. In the following, we make the conservative assumption that no measurement of EASs is performed if, in a region viewed by a PDM, there is at least one pixel which detects a light intensity which exceeds the average level by a factor of 3 or more. The average level of intensity essentially corresponds to the typical condition on oceans. With this assumption, the inefficiency of the instantaneous aperture is of $\sim$7 %. It is important to remember that Tatiana measurements [13], without focusing optics, indicate 2–3 times higher intensities in UV above big cities such as Mexico City and Houston compared to the average background level over the ocean. Moreover, in the presence of thick low-altitude clouds, it is possible to also measure in an area with anthropogenic light. This situation is not taken into account yet in the calculation, which has to be considered, therefore, conservative.

By adding together lightning, TLEs, and city light, the fraction of time in which JEM-EUSO is subject to transient or steady local sources of light is $f_{\rm loc} \sim 10$ %. Such effects reduce the effective instantaneous observational area to $1 - f_{\rm loc} \sim 90$ % of the geometrical one.

In order to quantify the reduction of the effective instantaneous aperture of the telescope due to the presence of clouds, a study on the distribution of clouds as a function of top altitude $H_{\rm C}$, optical depth $\tau_{\rm C}$ and geographical location are performed using several meteorological data sets [6, 20] obtaining similar results on the cloud occurrence. We summarize here the results obtained with the TOVS data set [21] as it allows the separation of the clouds in optical depths which is relevant for the determination of the exposure. A more detailed study and discussion of the JEM-EUSO observation in cloudy conditions is presented in [20]. Table 2 reports TOVS data with the occurrence of each cloud category during nighttime. The results apply

Table 2 Relative occurrence of clouds over the ISS orbit, taken from the TOVS database for nighttime, are presented as a matrix of cloud-top altitude vs optical depth for all locations

Cloud-top altitude $H_{\rm C}$	Optical depth $\tau_{\rm C}$			
	<0.1	0.1–1	1–2	> 2
	All data			
> 10 km	1.2 %	5.0 %	2.5 %	5.0 %
6.5–10 km	< 0.1 %	3.2 %	4.2 %	8.5 %
3.2–6.5 km	< 0.1 %	2.0 %	3.0 %	6.0 %
< 3.2 km	31 %	6.4 %	6.0 %	16 %

only to the region of the ISS trajectory and account for the residence time of the ISS as a function of latitude. Showers are simulated using ESAF according to the matrix of cloud occurrence determining the trigger efficiency in the different conditions, and obtaining the corresponding aperture. Results in Refs. [6, 20, 22] show the ratio κ_C between the aperture when the role of clouds is included, compared to purely clear atmosphere, for those events which have 'good quality' characteristics. Selecting the cases of clouds with $\tau_C < 1$, or shower maximum above the cloud-top altitude, i.e. $H_{max} > H_C$, κ_C is $\sim$ 72 % almost independently of energy.

4 Geometrical aperture in the nadir mode

The last parameter needed to estimate the aperture and the exposure is the trigger efficiency. The main objective of the trigger system is to reduce the rate of triggers due to background fluctuations to $\sim$0.1 Hz on FS imposed by downlink telemetry capabilities. The rejection level of the trigger algorithm determines the aperture of the instrument as a function of the energy. The rejection power also depends on the average night-glow background.

To estimate the geometrical aperture, a large number of proton showers are simulated by uniformly injecting them over an extended area $S_{sim} \gg S_{obs}$, where S_{obs} is the observed area by the main telescope, in a clear atmosphere condition with nominal background level of $I_{BG} = 500$ photons m^{-2} sr^{-1} ns^{-1}.

For N_{trig}, triggering samples among N_{sim} simulated EAS events with an energy E, the corresponding geometrical aperture $A(E)$ is defined by the following relation:

$$A(E) = \frac{N_{trig}}{N_{sim}} \cdot S_{sim} \cdot \Omega_0, \tag{1}$$

where $\Omega_0 = \pi$ sr is the solid angle acceptance for $0^\circ \leqslant \Theta \leqslant 90^\circ$.

By applying simple cuts on the distance R on the Earth's surface between the location of EAS impact and the projected point along the nadir direction, and on the lower limit in Θ, lower geometrical apertures are obtained.

Figure 3 shows the geometrical aperture as a function of energy for $H_{ISS} = 400$ km along with the apertures for different geometrical cuts in Θ and R, distance of core location on the Earth's surface from the center of FoV. In all the following figures, we refer to the simulated energies, not the reconstructed ones.

The geometrical aperture without geometrical cuts reaches the plateau[2] above $\sim (6-7) \times 10^{19}$ eV. At the highest energies, the geometrical aperture is close to saturation. The value is mainly determined by S_{obs} for a given H_{ISS} and, therefore, higher altitudes result in larger saturating apertures. Due to a minor contribution of EAS whose tracks are only partially contained in the FoV (those detected by the PDMs at the edges of the FoV), the geometrical aperture grows slightly with energy.

By applying the cut $\Theta > 60^\circ$, which reduces the solid angle acceptance to $\pi/4$ sr, a constant aperture is achieved above $\sim (4-5) \times 10^{19}$ eV. In addition, a more stringent

[2]It is defined by the condition in which the geometrical aperture is $> 0.8 \cdot S \cdot \Omega$ for the area S and solid angle acceptance Ω defined by specific geometrical cuts.

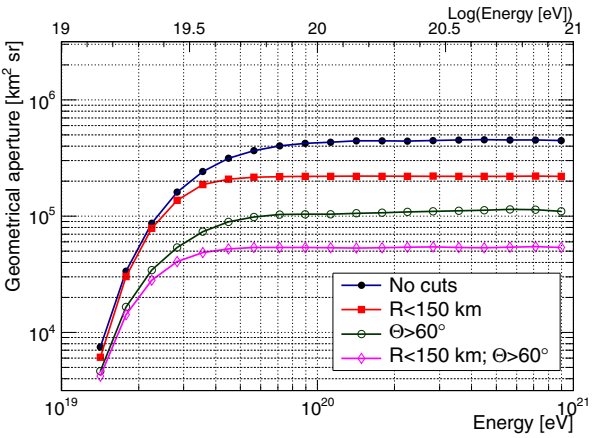

Fig. 3 Geometrical aperture as a function of energy. The filled circles and squares indicate geometrical apertures for the entire observation area and $R < 150$ km, respectively. The open circles and squares include a zenith angle cut of $\Theta > 60°$

cut with $R < 150$ km extends the constant aperture range down to $\sim 3 \times 10^{19}$ eV. The possibility to extend the plateau region at lower energies for a subset of events allows a cross-check of the flux measured by the full sample of events in the specific range of energies where the aperture of the instrument is not at the plateau level. Consequently, the overlapping energy range between JEM-EUSO and ground-based observatories is enlarged. This is due to the better performance of the optics in the central part of the FoV and to the higher number of photons collected by the telescope from more inclined showers (see Fig. 2). A more detailed discussion of these results is reported in Ref. [6].

Figure 4 shows the comparison of the geometrical aperture between proton and iron simulated showers without geometrical cuts. The aperture curve is essentially independent of the primary particle. The very minor displacement of the iron curve towards lower energies at a few percent level might be explained by the following reasons. The EAS observation from space has a better visibility of the early stages of the shower development compared to ground-based observation. Iron showers tend to cascade higher in atmosphere compared to proton ones and the apparent length of the EAS before impacting on the Earth's surface or on a cloud top is a bit longer. The difference in the relative scattering loss of light by a shift of ± 1 km in shower altitude which corresponds to a difference ~ 100 g cm^{-2} of atmospheric depth at shower maximum contributes to a difference of ~ 4 % in observed brightness for the considerations discussed in Section 2. Simulation results indicate that in the case of iron showers, a slightly higher number of photons reaches JEM-EUSO in comparison to proton showers with same energy and geometry. This results in the slight shift of the aperture curve at lower energies. In the following we will always refer to proton simulated showers, as both primaries give essentially the same aperture curve.

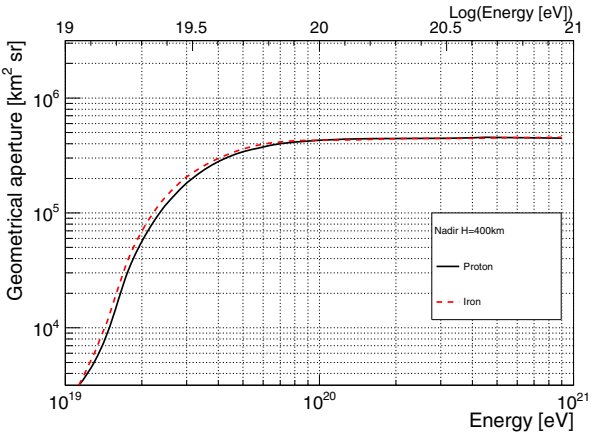

Fig. 4 Aperture as a function of energy at ISS altitude $H_{\mathrm{ISS}} = 400$ km without geometrical cuts: solid line for proton and dashed one for iron simulated events

5 Geometrical aperture in tilt mode

An interesting option for JEM-EUSO is the possibility of tilting the telescope. In the tilt mode, the observation area is scaled by $\propto (\cos\xi)^{-3}$ as a function of titling angle ξ of the optical axis from the nadir. This increases the sample of events at the highest energies and helps compensate for the reduction of the observation area in periods of lower orbiting altitudes. However, the larger distance under which showers appear, make them look dimmer. For this reason, the advantages of the tilt mode are not obvious by themselves and the improvement in exposure depends on the energy in a non-trivial way. Therefore, a devoted study must be performed to find a reasonable trade-off between increasing the exposure and keeping the threshold in energy at an acceptable level.

In the present study, a set of different tilting angles between 20° and 40° is simulated and compared to the nadir mode and first results obtained. It is important to underline that the analyses in which the optical axis is tilted by $\sim 0° - 25°$, can be easily assimilated to the nadir mode (defined in the following 'quasi-nadir mode'). In the case of even larger tilting angles ($\xi \gtrsim 25°$, tilt mode), a dedicated study is necessary to evaluate the performance in terms of the quality of the reconstructed events. This will be addressed in the future, in particular for the $\xi = 40°$ case where the observation area increases significantly and reaches the horizon. However, we report in the following first studies based on the trigger events for both quasi-nadir and tilt modes. They are based on the assumption of a standard ISS altitude of 400 km, and a more disfavored case, in which the ISS flies at 350 km. This second case is meant to indicate that lower altitudes allow for lowering the threshold in energy with a wider range of superposition with ground-based detectors, and that the loss in aperture in the nadir mode compared to the standard ISS altitude would be recovered at the highest energies by operating in the quasi-nadir mode.

Figure 5 shows the dependence of the observation area as a function of the tilting angle for $H_{\rm ISS} = 400$ km and 350 km. The area increases with ξ and becomes ~ 6 times larger than that of the nadir mode at $\xi = 40^\circ$ where a part of FoV sees the local horizon.

In order to estimate the aperture, a specific night-glow background has to be assumed. In the present work, the nominal background level of 500 photons m^{-2} sr^{-1} ns^{-1} is assumed to be constant over the entire FoV. Most likely, this is a too simplistic assumption since the background radiance depends on the tilting angle under which the atmosphere is observed. However, at a first-order approximation and especially for low tilting angles we can consider the shower-to-detector distance to be the leading factor affecting the threshold in energy. In fact, the shower signal can be expected to decrease proportionally to the inverse square of the distance which is much stronger than any reasonable increase of the background rate as a function of the tilting angle. Moreover, the increase of the background level corresponds to an increase of the threshold in energy proportional to $\sqrt{I_{\rm BG}}$. On the other hand, the signal variations linearly affect the threshold. Efforts are ongoing for a more careful estimation of the background dependence as a function of the tilting angle.

Figure 6 shows the aperture as a function of energy for different tilting angles. The ISS altitude $H_{\rm ISS} = 400$ km and no geometrical cuts are assumed. As expected by tilting the telescope, the threshold in energy increases, as well, as the aperture at the highest energies. The quasi-nadir configuration of $\xi = 20^\circ$ allows an almost constant aperture to be kept at the lowest energies, while increasing it moderately at $\sim 10\ \% - 20\ \%$ level in $E \gtrsim 10^{20}$ eV. Compared to nadir mode, the tilt one is suitable to increase the aperture at the energies $E \gtrsim 2 \times 10^{20}$ eV where the flux is particularly low, reaching a factor of $\sim$ 1.8 higher aperture at $E > 5 \times 10^{20}$ eV for the $\xi = 30^\circ$ case. On the right, the corresponding annual exposure is shown (see Section 6 for discussion).

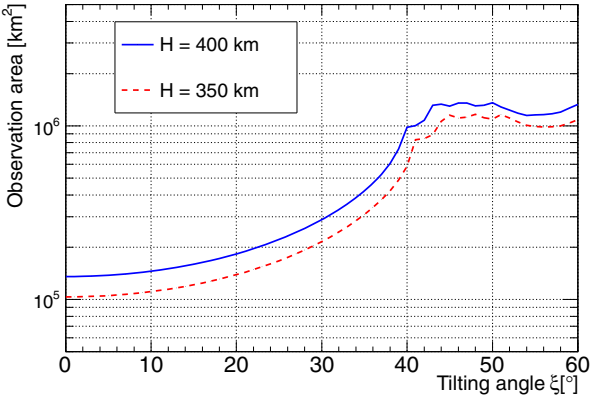

Fig. 5 The JEM-EUSO observation area are shown as a function of the tilting angle for ISS altitude 400 km and 350 km. The tilting angle of $\xi \sim 40^\circ$ at which the edge of the FoV reaches the horizon is indicated as well

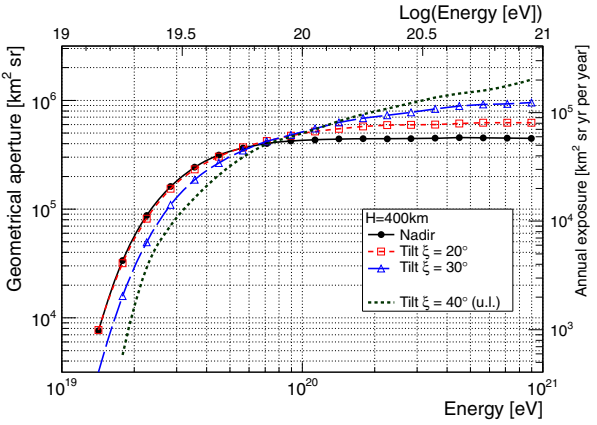

Fig. 6 JEM-EUSO aperture as a function of energy for different tilting angles. $H_{\rm ISS} = 400$ km and no geometrical cuts are assumed. On the right, the corresponding yearly growth in exposure is shown (see Section 6). In the case of $\xi = 40°$, the dashed line shows the upper limit (u.l.) on the reachable aperture and exposure

The aperture in tilt mode tends to continuously grow with energy compared to the nadir or quasi-nadir mode. This is due to the fact that higher luminosities are required to trigger PDMs in the furthest regions of the FoV. During the data taking in the mission, the proper understanding of the growth of the aperture with energy will be verified experimentally by comparing the measured fluxes in nadir and tilted modes in the range of 5×10^{19} eV $\lesssim E \lesssim 2\times10^{20}$ eV where both modes provide comparable statistics. Moreover, the tilt mode monitors part of its FoV in similar conditions as in nadir mode. In the case of $\xi = 30°$ tilt angle, half of the FoV seen in nadir mode belongs to the FoV of the tilt one, therefore, the quality of shower reconstruction is similar. On the other hand, the expected number of events at $E \gtrsim 2 \times 10^{20}$ eV detected by JEM-EUSO in nadir mode varies in 1–10 per year, depending on assumed UHECR fluxes by the Pierre Auger Observatory [23] or Telescope Array [24].

Figure 7 shows JEM-EUSO aperture as a function of energy in nadir mode for $H_{\rm ISS} = 400$ km and 350 km as well as the aperture in quasi-nadir mode for $\xi = 25°$ for $H_{\rm ISS} = 350$ km. Thanks to the higher trigger efficiency for $H_{\rm ISS} = 350$ km configuration in nadir mode, the same aperture of the standard configuration is guaranteed at the lowest energies. Above 10^{20} eV the aperture can be recovered by the quasi-nadir configuration. Only a moderate loss of aperture below ~ 20 % level in the range of 3×10^{19} eV $< E < 10^{20}$ eV remains. However, this is the region where the acquired statistics are relatively high.

6 Exposure

From the above results, the exposure per year of operation, defined as the 'annual exposure', is evaluated as a function of energy:

$$\text{(Annual exposure)} \equiv A(E) \cdot \kappa_{\rm C} \cdot \eta_0 \cdot (1 - f_{\rm loc}) \cdot (1\ [\text{yr}]). \qquad (2)$$

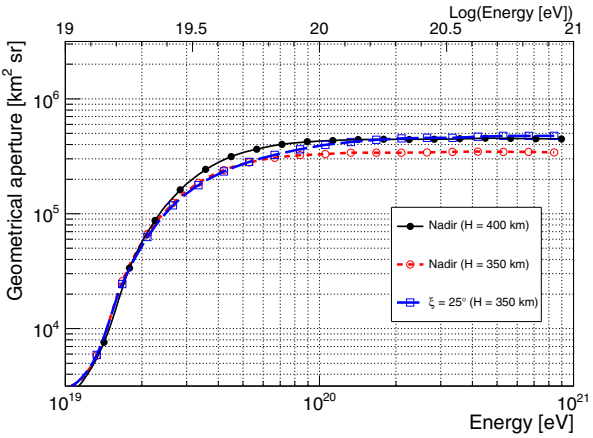

Fig. 7 JEM-EUSO aperture as a function of energy for nadir mode at $H_{\mathrm{ISS}} = 400$ km and 350 km as well as that for quasi-nadir mode wtih $\xi = 25°$ at $H_{\mathrm{ISS}} = 350$ km. All plots refer to the one without geometrical cuts

In this estimation, we use $\kappa_{\mathrm{C}} = 72$ %, $\eta_0 = 20$ %, and $f_{\mathrm{loc}} = 10$ %, respectively and independently of the tilting angle. With the conditions assumed in the present work, the overall conversion factor from geometrical aperture to exposure is about ~ 0.13 yr. In reality, it is expected that the cloud inefficiency will be lower for the tilting mode. This is due to the fact that the PDMs looking at farther distances are more efficient in detecting inclined showers that develop in higher atmospheric levels and deliver more light to the telescope (see Fig. 2). Therefore, the cloud inefficiency is less important. On the other hand, the effect of local light sources will be more pronounced because the FoV of such PDMs is larger. These two factors compensate each other at a first-order approximation, however, a dedicated study will be conducted in the future to estimate the second-order effects. The inefficiencies related to

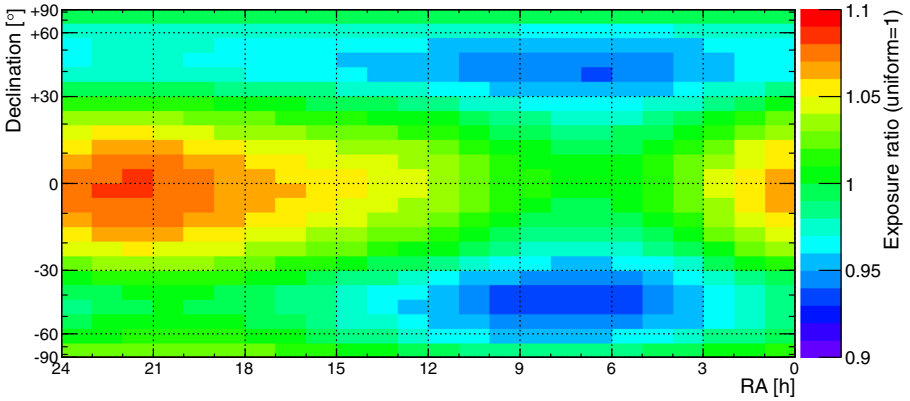

Fig. 8 Expected distribution of observed exposure as a function of declination and right ascension. Clear and cloudy atmosphere are considered

Table 3 Arrival direction determination error for different energies and shower zenith angles Θ

Energy	Arrival direction determination error at 68 % CL			
[eV]	Θ = 30°	Θ = 45°	Θ = 60°	Θ = 75°
5×10^{19}	4.5°	4.0°	2.7°	1.3°
1×10^{20}	4.2°	2.7°	1.8°	0.8°
3×10^{20}	3.5°	1.8°	0.9°	0.6°

the operation of the telescope lid, detector maintenance or aging of MAPMTs, etc. and the ISS operation, such as rockets docking, are not taken into account yet. The fraction of the triggered events that are reconstructed and the quality of such events is described in detail in Refs. [9, 10]. The present results constitute an upper limit on the effective exposure of the instrument for the assumed conditions for ξ = 0°, 20°, 30°, etc.

On the right axis of Fig. 6, the scale for the annual exposure is shown for the geometrical apertures indicated in the figure. For the nadir mode, the JEM-EUSO annual exposure without geometrical cuts around 10^{20} eV is expected to be $\sim$ 9 times larger than that of Auger of 7000 km^2 sr yr as given in [25], and more than 50 times of the annual exposure of TA [26]. In the tilt mode, the exposure further increases at extreme energies by another factor of $\sim$2.

Unlike ground-based observatories, the global ISS orbit and better sensitivities for EAS with large zenith angles allows observation of the entire celestial sphere. The exposure distribution has only limited anisotropies in declination and right ascension which are due to the different resident time of the ISS as a function of the latitude, to the different twilight time for different latitudes and to local and seasonal dependence of the cloud distribution and local man-made light.

Figure 8 summarizes the results when all the above effects are taken into account. The global distribution of clouds is assumed from the analysis of TOVS data in Ref. [20]. The exposure distribution over the celestial sphere is rather uniform within $\pm$10 % level.

7 Discussion and conclusions

The exposure discussed in this work are based on the trigger efficiencies, as described in this paper and in Ref. [6], and on the request that the shower maximum is visible. The obtained results have to be considered as the potential of the JEM-EUSO experiment. The quality of event reconstruction is an additional parameter that has to be defined specifically for each type of analysis. Even though a detailed simulation is necessary to clarify how the different atmospheric conditions affect the quality of the event reconstruction, and this is currently in progress, we report in the following a few typical examples. The presence of an optically thin cloud at high altitudes, if not properly taken into account, most probably causes a lower estimation of the event energy, however, the angular reconstruction is almost unaffected. This means

that such an event should not be used for the determination of the energy spectrum but can be used for source identification analysis. The presence of an optically thick cloud below $\sim$ 3 km slightly shortens the shower track but does not have major implications in the energy reconstruction for most of the EAS zenith angles as the shower maximum is located at higher altitudes. Indeed, works in the past demonstrated the feasibility of reconstructing EAS with acceptable uncertainty even in the presence of clouds [1, 11].

The current status of the quality of JEM-EUSO event reconstruction in clear atmosphere condition is reported in the following, while details of the analyses are discussed in Refs. [9, 10]. The arrival direction determination error at 68% confidence level (CL) is summarized in Table 3 which includes all triggered events without selection cut applied to the data. For the case of 10^{20} eV energy and $\Theta = 60^{\circ}$ zenith angle showers, more than 95 % of the triggered showers are reconstructed. This is due to the stringent telemetry budget of JEM-EUSO, which allows a trigger rate of $\sim$0.1 Hz, and requires an already severe quality-based selection of the events on board. This is a distinct property from the ground-based UHECR experiments where, typically, the data rate is not a major concern, and the quality-based selection is operated offline.

The role of clouds needs to be assessed with dedicated simulations. However, general rules can be derived from simple considerations. In the following, we present two relatively bad situations. The first one is an optically thin cloud at 10–15 km altitude with moderately high optical depth such as $\tau_C = 0.7$, which is one the critical cloudy situations for EAS observation from space. Such a cloud reduces the shower brightness B observed by JEM-EUSO, compared to the clear atmosphere case B_0, to $B_0 \cdot \exp(-0.7) \sim B_0/2$ [22]. This means that at a first-order approximation, the quality of a 10^{20} eV event reconstruction in such a cloudy atmospheric condition will resemble to the observation of a 5×10^{19} eV EAS with a similar zenith angle in clear atmosphere. As a second example, we consider an optically thick clouds, such as $\tau_C > 5$, whose top is located at 6–7 km altitude. Such a cloud blocks the observation of the shower below it. By looking at Fig. 2, the visible portion of the track of a 60° zenith angle shower is comparable to the 30° case of the same energy in clear atmosphere (see Table 3). As $\kappa_C = 0.72$ factor is included in the exposure, the location of the shower maximum above cloud-top is already taken into account, therefore the 60° zenith angle shower is the worst acceptable case in that specific cloud scene.

In the case of the tilt mode, it is even more difficult to derive some reference numbers without a proper simulation. Nevertheless, the observation of an event at energy $E > 5 \times 10^{20}$ even with 10° angular resolution would be already useful to evaluate where it is compatible or not with one of the sources that might have been discovered at lower energies.

Regarding the quality of energy reconstruction, results presented in Ref. [10] in the case of clear atmosphere, indicate that when taking into account all FoV and all zenith angles, the energy resolution is better than $\pm$30 % at 68 % CL for energies above $\sim 7 \times 10^{19}$ eV, when accepting the best 85 % of the events based on quality cuts. The same level of resolution can be achieved at lower energies if quality cuts are applied on the reconstructed shower profile.

Simulations are on going to estimate the performance in case of cloudy atmosphere. In the presence of optically thin clouds at high altitudes, the energy estimation will be lower than the true one if no correction for the light attenuation is performed. This is safe for the source identification analysis which is done using all events above a threshold energy. The key point is the identification of the presence of clouds, even though the optical depth could not be retrieved. In the presence of optically thick clouds at low altitudes, the shower track will be shorter. However, as far as the shower maximum is clearly identified, the energy estimation will be retrieved, in most cases, from the the light intensity at shower maximum.

Regarding the tilt mode, the event triggering at distances $R > 400$ km automatically identifies events with energy $E > 5 \times 10^{19}$ eV. Assuming again a null knowledge of the location of the shower maximum in atmosphere, except $H_{\max}$ being in the range of 7 ± 5 km, for an EAS located in the direction of 60° away from the nadir, an uncertainty of only 40% due to the scattering loss of light in atmosphere on the brightness of the EAS is derived. A null detection of events with energy $E > 3 \times 10^{20}$ eV, which is the maximum energy detected so far, will set an upper limit in flux of about one order of magnitude lower than what has been reached up to now.

Summarizing the results on the exposure, simulations show that JEM-EUSO reaches almost full efficiency in the nadir mode already at energies around 3×10^{19} eV for a restricted subset of events, and provides full aperture at energies $E > (6 - 7) \times 10^{19}$ eV. The expected exposure is essentially independent of the incident primary particle. The observational duty cycle and the role of clouds are summarized. The expected annual exposure of JEM-EUSO in the nadir mode around 10^{20} eV is equivalent to about 9 years exposure of Auger and more than 50 years exposure of TA.

The quasi-nadir mode with $\xi \lesssim 25°$ allows a slight increase in the exposure at $E \gtrsim 10^{20}$ eV. This is an interesting option to recover the exposure from unexpected operational inefficiencies or low ISS altitudes. A first study on the tilt mode is presented. The aperture is expected to increase by a factor of $\sim$2 for a tilting angle $\xi \sim 30°$ compared to the nadir mode at the highest energies. However, this result has to be confirmed by further analyses including event reconstruction.

Thanks to the ISS orbit, JEM-EUSO surveys the entire celestial sphere with a very limited non-uniformity of the exposure at $\sim$ 10 % level at on declination and right ascension, taking into account coverage distribution and seasonal variation of the clouds.

Acknowledgments This work was partially supported by Basic Science Interdisciplinary Research Projects of RIKEN and JSPS KAKENHI Grant (22340063, 23340081, and 24244042), by the Italian Ministry of Foreign Affairs - General Direction for the Cultural Promotion and Cooperation, by the Deutsches Zentrum fuer Luft- und Raumfahrt, by the 'Helmholtz Alliance for Astroparticle Physics HAP' funded by the Initiative and Networking Fund of the Helmholtz Association (Germany), and by Slovak Academy of Sciences MVTS JEM-EUSO as well as VEGA grant agency project 2/0076/13.

References

1. Takahashi, Y., et al.: (JEM-EUSO Coll.), the JEM-EUSO Mission. New J. Phys. **11**, 065009/1-21 (2009)

2. Adams Jr., J.H., et al.: (JEM-EUSO Coll.) an overview of the JEM-EUSO instrument. This volume
3. Greisen, K.: End to the cosmic-ray spectrum? Phys. Rev. Lett. **16**, 748–750 (1966)
4. Zatsepin, G.T., Kuz'min, V.A.: Upper limit of the spectrum of cosmic rays. J. Exp. Theor. Phys. Lett. **4**, 78–80 (1966)
5. Adams Jr., J.H., et al.: (JEM-EUSO Coll.) ultra high energy photons and neutrinos with JEM-EUSO. This volume
6. Adams Jr., J.H., et al.: (JEM-EUSO Coll.), an evaluation of the exposure in nadir observation of the JEM-EUSO mission. Astropart. Phys. **44**, 76–90 (2013)
7. Adams Jr., J.H., et al.: (JEM-EUSO Coll.) the AM system of the JEM-EUSO instrument. This volume
8. Wiencke, L., et al.: (JEM-EUSO Coll.) the JEM-EUSO global light system. In: Proceedings 33^{rd} International Cosmic Ray Conference, #818 (2013)
9. Adams Jr., J.H., et al.: (JEM-EUSO Coll.) performances of JEM-EUSO: Angular reconstruction. This volume
10. Adams Jr., J.H., et al.: (JEM-EUSO Coll.) performances of JEM-EUSO: Energy and X_{max} reconstruction. This volume
11. Abu-Zayyad, T., Jui, C.C.H., Loh, E.C.: The effect of clouds on air showers observation from space. Astropart. Phys. **21**, 163–182 (2004)
12. Berat, C., et al.: Full simulation of space-based extensive air showers detectors with ESAF. Astropart. Phys. **33**(4), 221–247 (2010)
13. Garipov, G.K., et al.: UV radiation from the atmosphere: Results of the MSU Tatiana satellite measurements. Astropart. Phys. **24**, 400–408 (2005)
14. Barbier, M., et al.: NIGHTGLOW: An instrument to measure the Earth's nighttime ultraviolet glow - results from the first engineering flight. Astropart. Phys. **22**, 439–449 (2005)
15. Catalano, O., et al.: The atmospheric nightglow in the 300 - 400 nm wavelength: Results by the balloon-borne experiment BABY. Nucl. Inst. Methods A **480**, 547–554 (2002)
16. Mernik, T., Bobik, P., Putis, M., et al.: (JEM-EUSO Collaboration), UV night background estimation in South Atlantic Anomaly. In: Proceedings of 33rd International Cosmic Ray Conference. ID0874 (2013). arXiv:1307.7071
17. Heinderickx, B., Quaghebeur, B., Speelman, E., et al.: Spacecraft charging models in ESA's SPace ENVironment Information System (SPENVIS), spacecraft charging technology. In: Proceedings of the 17th International Conference, European Space Agency. ESA SP-476, pp. 163–168 (2001)
18. Agostinelli, S., Allison, J., Amako, E., et al.: GEANT4 – a simulation toolkit. Nucl. Inst. Methods A **506**, 250–303 (2003)
19. http://www.swpc.noaa.gov/Aurora/index.html (2013)
20. Adams Jr., J.H., et al.: (JEM-EUSO Coll.), JEM-EUSO observation in cloudy conditions. This volume
21. TOVS. http://www.ozonelayer.noaa.gov/action/tovs.htm/ (2008)
22. Sáez-Cano, G., Shinozaki, K., del Peral, L., et al.: Observation of extensive air showers in cloudy conditions by the JEM-EUSO Space Mission, to appear on Advances in Space Research (2013). doi:10.1016/j.asr.2013.07.015
23. Settimo, M.: For the Auger collaboration, measurement of the cosmic ray energy spectrum using hybrid events of the Pierre Auger observatory. Eur. J. Suppl. Plus **127**, 87 (2012)
24. Dawson, B.R., et al.: The energy spectrum of cosmic rays at the highest energies. EPJ Web Conf. **53**, 01005 (2013)
25. Abraham, J., et al.: (Auger Coll.), trigger and aperture of the surface detector array of the Pierre Auger observatory. Nucl. Inst. Methods A **613**, 29–39 (2010)
26. Abu-Zayyad, T., et al.: (Telescope Array Coll.), the surface detector array of the Telescope Array experiment. Nucl. Inst. Methods A **689**, 87–97 (2012)